J. Fluid Mech. (2002), *vol.* 471, *pp.* 339–363.
DOI: 10.1017/S0022112002001878 Printed in the United Kingdom

Stability of thermal convection in two superimposed miscible viscous fluids

By MICHAEL LE BARS AND ANNE DAVAILLE

Laboratoire de Dynamique des Systèmes Géologiques, Institut de Physique du Globe de Paris
CNRS, UMR 7579, 4 Place Jussieu, 75 252 Paris cedex 05, France

(Received 5 November 2001 and in revised form 25 March 2002)

The stability of two-layer thermal convection in high-Prandtl-number fluids is investigated using laboratory experiments and marginal stability analysis. The two fluids have different densities and viscosities but there is no surface tension and chemical diffusion at the interface is so slow that it is negligible. The density stratification is stable. A wide range of viscosity and layer depth ratios is studied. The onset of convection can be either stationary or oscillatory depending on the buoyancy number B, the ratio of the stabilizing chemical density anomaly to the destabilizing thermal density anomaly: when B is lower than a critical value (a function of the viscosity and layer depth ratios), the oscillatory regime develops, with a deformed interface and convective patterns oscillating over the whole tank depth; when B is larger than this critical value, the stratified regime develops, with a flat interface and layers convecting separately. Experiments agree well with the marginal stability results. At low Rayleigh number, characteristic time and length scales are well-predicted by the linear theory. At higher Rayleigh number, the linear theory still determines which convective regime will start first, using local values of the Rayleigh and buoyancy numbers, and which regime will persist, using global values of these parameters.

1. Introduction

In contrast to the Rayleigh–Bénard problem for one fluid, instability in two chemically stratified fluid layers can be either steady or oscillatory (Richter & Johnson 1974), as for the closely related and well-documented case of double-diffusive convection (e.g. Veronis 1968; Turner 1979; Hansen & Yuen 1989). But the number of parameters involved in this problem is large and there exists no comprehensive picture of the domains in which a given regime prevails.

The steady case, where the interface remains flat and convection develops in two superimposed layers, has been extensively studied, because of its suggested occurrence in the Earth's mantle (Richter & McKenzie 1981; Busse 1981; Cserepes & Rabinowicz 1985; Ellsworth & Schubert 1988; Cserepes, Rabinowicz & Rosemberg-Borot 1988; Sotin & Parmentier 1989). Rasenat, Busse & Rehberg (1989) showed that an oscillatory two-layer regime could also develop, involving no deformation of the interface, with a convective pattern oscillating between viscous and thermal coupling: experimental studies of this configuration has been performed by Busse & Sommermann (1996) and Andereck, Colovas & Degen (1996). However, studies of the oscillatory regime where the interface deforms and convection develops over the whole depth of the tank have been limited to cases where the physical properties of the two fluids (viscosity, thermal diffusivity, thermal expansivity) are equal (Richter

& Johnson 1974; Schmeling 1988) or nearly equal (Renardy & Joseph 1985; Renardy & Renardy 1985).

One question that remains open is the fate of the oscillatory regime when the viscosity contrast between the two layers varies by several orders of magnitude. The answer to this question could provide valuable insight into the dynamics of the Earth's mantle where large viscosity variations are expected and the type of convection ('two-layered' or 'whole-mantle') is still controversial (Olson, Silver & Carlson 1990; Tackley 2000). Motivated by this geophysical interest, laboratory experiments have recently been performed to investigate the influence of the viscosity contrast on two-layer thermal convection at high Rayleigh and Prandtl numbers (Davaille 1999*a*, *b*; Le Bars & Davaille, in preparation). The two fluids were miscible in the sense that there was no surface tension at the interface. Depending on the buoyancy number B, the ratio of the stabilizing chemical density anomaly to the destabilizing thermal density anomaly, two regimes were observed: for $B > 1$, thermal convection develops in two superimposed layers, separated by a thermal boundary layer at a relatively undeformed interface, while for $B < 0.35 - 0.55$, the interface deforms in large domes which move up and down quasi-periodically.

Here, we use marginal stability analysis and laboratory experiments to investigate further the stability and occurrence of the two thermochemical regimes, as a function of the viscosity, depth and density ratios between the two fluids: our purpose is to determine for each case the onset of convection and the prevailing regime. Section 2 sets up the problem formally and presents the results of the marginal stability analysis. In § 3, these results are first compared with experiments at low Rayleigh number, and then used to determine the stability of two-layer systems at higher Rayleigh number.

2. Marginal stability analysis

2.1. *Analytical formulation*

In the two-dimensional x, z space, we consider two superimposed layers of fluids, respectively of densities ρ_{1_0} and ρ_{2_0}, kinematic viscosities ν_1 and ν_2 (dynamic viscosities η_1 and η_2), and depth d_1 and d_2 (figure 1*a*). Only the case where the density stratification is stable is studied, so that the heavier fluid is at the bottom. All the physical properties of the two fluids are taken to be equal, except their densities and viscosities. There is neither surface tension nor chemical diffusion at the interface between the two fluids. The lower and upper planes are held at uniform temperatures T_1 and T_2 respectively. Each plane is assumed to be a perfect thermal conductor, and the kinematic condition on those boundaries is either traction-free, for comparison with previous work, or rigid (zero horizontal velocity) for comparison with the experiments. Unless specified, numerical values presented in this paper are for rigid boundaries.

To non-dimensionalize the problem, we use the length scale $d = d_1 + d_2$, the total thickness of fluid, and the temperature scale $\Delta T = T_1 - T_2$, the total temperature difference. In this study, we aim to determine the occurrence of the oscillatory regime, where the interface deforms in large domes (Davaille 1999*b*): we thus choose a velocity scale characteristic of this problem, namely the Stokes velocity of a dome developing from layer 1 into layer 2: $v = \alpha g \Delta T d^2/\nu_2$, where α is the thermal expansivity and g the acceleration due to gravity. The time scale is given by $d/v = \nu_2/\alpha g \Delta T d$, and the viscous pressure scale by $\eta_2 v/d = \alpha \rho_{2_0} g \Delta T d$. In the following, all the variables are non-dimensionalized using these scales.

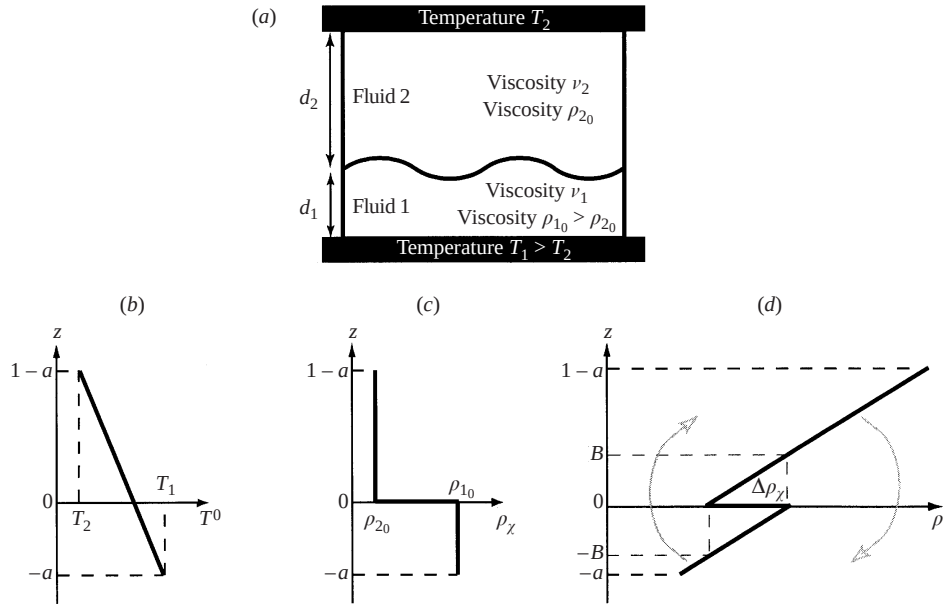

FIGURE 1. Configuration of the problem: (*a*) set-up, (*b*) linear temperature profile, (*c*) chemical density profile and (*d*) effective density profile, taking into account thermal and chemical effects.

We study the linear stability of the static solution, which exhibits a linear temperature profile (figure 1*b*):

$$T = \frac{T_1}{\Delta T} - (z + a), \tag{2.1}$$

where $a = d_1/d$. Let θ_i and p_i be the deviations of the temperature and pressure from their static distribution, and $\boldsymbol{u}_i$ be the velocity vector. Assuming that thermal effects and chemical density contrast are small, the fluids are considered incompressible, except for buoyancy terms (Boussinesq approximation). In a first-order approximation, the equation of state used within each layer i is thus

$$\rho_i(T) = \rho_{i_0} - \alpha\rho_0(T\Delta T - T_0), \tag{2.2}$$

where $\rho_0 = (\rho_{1_0} + \rho_{2_0})/2$. We obtain for each layer i a dimensionless form of the equations governing the motion:

$$\nabla \cdot \boldsymbol{u}_i = 0, \tag{2.3}$$

$$\frac{Ra}{Pr}\left(\frac{\partial}{\partial t} + \boldsymbol{u}_i \cdot \nabla\right)\boldsymbol{u}_i = -\nabla p_i + \theta_i \boldsymbol{k} + \frac{\nu_i}{\nu_2}\nabla^2 \boldsymbol{u}_i, \tag{2.4}$$

$$Ra\left[\left(\frac{\partial}{\partial t} + \boldsymbol{u}_i \cdot \nabla\right)\theta_i - \boldsymbol{u}_i \cdot \boldsymbol{k}\right] = \nabla^2\theta_i. \tag{2.5}$$

The vertical unit vector $\boldsymbol{k}$ is directed opposite to gravity. The Rayleigh and Prandtl numbers are defined by

$$Ra = \frac{\alpha g \Delta T d^3}{\kappa \nu_2} \quad \text{and} \quad Pr = \frac{\nu_2}{\kappa},$$

where κ is the thermal diffusivity. We also define the viscosity ratio between the two layers $\gamma = \nu_1/\nu_2$. Since we are interested in the onset of infinitesimal disturbances,

the nonlinear terms $(\boldsymbol{u}_i \cdot \nabla)\boldsymbol{u}_i$ and $(\boldsymbol{u}_i \cdot \nabla)\theta_i$ are negligible. Furthermore, we restrict our attention to the case of infinite Prandtl number, relevant to the Earth's mantle. Then, taking twice the curl of (2.4), and using (2.5) to eliminate the temperature, one obtains for the vertical velocity w_i:

$$\left(Ra\frac{\partial}{\partial t} - \nabla^2\right)\nabla^4 w_1 = -\frac{Ra}{\gamma}\frac{\partial^2 w_1}{\partial x^2}, \tag{2.6a}$$

$$\left(Ra\frac{\partial}{\partial t} - \nabla^2\right)\nabla^4 w_2 = -Ra\frac{\partial^2 w_2}{\partial x^2}. \tag{2.6b}$$

The outer boundary conditions are in each layer ($z = -a$ and $z = 1 - a$):

$$w = \frac{\partial w}{\partial z} = 0 \text{ for a rigid boundary,} \tag{2.7a}$$

$$w = \nabla^2 w = 0 \text{ for a free boundary,} \tag{2.7b}$$

and $\theta = 0$ which yields

$$\nabla^4 w = 0. \tag{2.8}$$

The equilibrium position of the interface between the fluids is assumed to be $z = 0$. Distortions of the interface from this position are described by the function $h(x, t)$. Assuming that those distortions are small, a Taylor expansion around $z = 0$ is used to obtain the linearized interfacial conditions (see Joseph & Renardy 1993 for the complete derivation):

The kinematic condition for the material interface yields

$$w_1 = \frac{\partial h}{\partial t}. \tag{2.9}$$

Continuity of velocity and incompressibility yield

$$w_1 = w_2, \tag{2.10}$$

$$\frac{\partial w_1}{\partial z} = \frac{\partial w_2}{\partial z}. \tag{2.11}$$

Continuity of shear stress yields

$$\gamma\frac{\partial^2 w_1}{\partial z^2} - \frac{\partial^2 w_2}{\partial z^2} = \gamma\frac{\partial^2 w_1}{\partial x^2} - \frac{\partial^2 w_2}{\partial x^2}. \tag{2.12}$$

Continuity of normal stress yields

$$p_1 - 2\gamma\frac{\partial w_1}{\partial z} = p_2 - 2\frac{\partial w_2}{\partial z} + Bh, \tag{2.13a}$$

where B is the buoyancy number, the ratio of the stabilizing chemical density anomaly to the destabilizing thermal density anomaly:

$$B = \frac{\rho_{1_0} - \rho_{2_0}}{\alpha\rho_0\Delta T}.$$

Taking $\partial^3/\partial t\partial x^2$ of (2.13a) and eliminating p_i with (2.4) and h with (2.9), we obtain

$$\nabla^2\frac{\partial^2}{\partial t\partial z}(\gamma w_1 - w_2) + 2\frac{\partial^4}{\partial t\partial z\partial x^2}(\gamma w_1 - w_2) = -B\frac{\partial^2 w_1}{\partial x^2}. \tag{2.13b}$$

Continuity of temperature yields

$$\theta_1 = \theta_2 \Rightarrow \gamma \nabla^4 w_1 = \nabla^4 w_2. \tag{2.14}$$

Continuity of heat flux yields

$$\frac{\partial \theta_1}{\partial z} = \frac{\partial \theta_2}{\partial z} \Rightarrow \gamma \nabla^4 \frac{\partial w_1}{\partial z} = \nabla^4 \frac{\partial w_2}{\partial z}. \tag{2.15}$$

Because we used a scaling characteristic of interface deformation, the buoyancy number B appears in (2.13). Other studies using the classical thermal diffusive scaling (Richter & Johnson 1974; Joseph & Renardy 1993) lead to the appearance of R_s, Rayleigh number based on the chemical density difference:

$$R_s = \frac{(\rho_{1_0} - \rho_{2_0}) g d^3}{\kappa \eta_2}. \tag{2.16}$$

These two numbers are simply linked by the relation

$$R_s = Ra B. \tag{2.17}$$

Analysing the problem in terms of normal modes, the solution is sought in the form

$$w(x, z, t) = W(z) \exp(\mathrm{i}kx + st) \text{ with } s = \sigma + \mathrm{i}\omega. \tag{2.18}$$

Hence, $W(z)$ is solution of the following equations:

for $0 \geqslant z \geqslant -a$,

$$(sRa + k^2 - \mathrm{D}^2)(\mathrm{D}^2 - k^2)^2 W_1 = k^2 \frac{Ra}{\gamma} W_1, \tag{2.19a}$$

for $1 - a \geqslant z \geqslant 0$,

$$(sRa + k^2 - \mathrm{D}^2)(\mathrm{D}^2 - k^2)^2 W_2 = k^2 Ra W_2, \tag{2.19b}$$

where D stands for $\mathrm{d}/\mathrm{d}x$. The general solution of (2.19) is

for $0 \geqslant z \geqslant -a$,

$$W_1 = \sum_{1 \leqslant j \leqslant 3} A_{1j} \exp(q_{1j}(a + z)) + B_{1j} \exp(-q_{1j}(a + z)), \tag{2.20a}$$

for $1 - a \geqslant z \geqslant 0$,

$$W_2 = \sum_{1 \leqslant j \leqslant 3} A_{2j} \exp(q_{2j}(1 - a - z)) + B_{2j} \exp(-q_{2j}(1 - a - z)). \tag{2.20b}$$

The coefficients q_{ij} are solutions of the equations:

for $0 \geqslant z \geqslant -a$,

$$(sRa + k^2 - q_{1j}^2)(q_{1j}^2 - k^2)^2 = \frac{Ra}{\gamma} k^2, \tag{2.21a}$$

for $1 - a \geqslant z \geqslant 0$,

$$(sRa + k^2 - q_{2j}^2)(q_{2j}^2 - k^2)^2 = Ra k^2, \tag{2.21b}$$

and the twelve constants A_{ij} and B_{ij} are determined by the six matching conditions at the interface (2.10)–(2.15) and the six outer boundary conditions (2.7)–(2.8). Those conditions represent an homogeneous system of equations for A_{ij} and B_{ij}. Non-zero solutions exist if the determinant of the coefficient matrix (given in the Appendix) vanishes. The system thus represents a transcendental equation relating a, γ, B, Ra, k

and complex s, that must be solved numerically. Since the problem defined above is not self-adjoint, the determinant and the eigenvalues can be complex, and the onset of convection can be oscillatory as well as stationary. Moreover, the equations are identical on interchanging (γ, a) and $(1/\gamma, 1-a)$. So only results for $\gamma \geqslant 1$ will be presented, which means that the lower layer will always be the more viscous. This is also the situation encountered in our laboratory experiments.

2.2. *Results for marginal stability*

Looking for the marginal stability, we assume that $\sigma = 0$ and thus s reduces to $i\omega$. For fixed values of the parameters a, γ and B, the roots of the determinant are sought in the (k, ω, Ra) space, using the Nelder–Mead simplex method (Nelder & Mead 1965). In each case, the critical Rayleigh number is the minimum value of Ra as the wavenumber k is varied.

2.2.1. *Accuracy of the method*

The convergence of the computer code was checked for the case $\gamma = 1$. For layers of equal properties, there are two situations identical to the classical Rayleigh–Bénard problem in one fluid. The eigenvalues for those cases are real, and given by Chandrasekhar (1961):

(a) when there is no density jump at the interface ($B = 0$), convection occurs throughout the whole layer with $Ra_c = 657.51$ and $k = 2.22$ for free boundaries and $Ra_c = 1707.76$ and $k = 3.12$ for rigid boundaries;

(b) when $a = 0.5$, the most unstable two-layer mode, which has zero vertical velocity at the interface, corresponds in each layer to Rayleigh–Bénard convection with a free boundary condition at the interface; it occurs, with our notation, at $Ra_c = 10520.16$ and $k = 4.43$ for free boundaries, and at $Ra_c = 17610.39$ and $k = 5.365$ for rigid boundaries (corresponding respectively to $Ra_c = 657.51$ and $Ra_c = 1100.65$ if the characteristic scales are taken to be those of one layer).

The more general case encountered throughout the (B, Ra) parameter space for $\gamma = 1$ and $a = 0.5$ has already been solved by Richter & Johnson (1974) for free boundaries. There, the eigenvalues are either real or complex, producing respectively either steady stratified convection or oscillatory instabilities. Our computer code reproduces exactly their numerical results.

2.2.2. *Dependence on B*

Figure 2 shows the stability diagram of the system for a given (γ, a) and figure 3 the corresponding interface velocity, horizontal wavelength ($\lambda = 2\pi/k$) and temporal frequency. Depending on B, instability sets in under two different regimes:

(a) Stratified regime: for B greater than a critical value $B_c(\gamma, a)$, the most unstable mode has a zero vertical velocity at the interface (figure 3a); convection develops above and below the interface with a wavelength comparable to one layer depth (figure 3b); motions are steady (figure 3c). The interface remains at its equilibrium position $h = 0$, and the stability of the stratified regime is independent of B (figure 2), as expected from (2.13a). The vertical velocity is maximum in the less viscous fluid, whereas in the other fluid motions are delayed and much slower: the less viscous layer is thus active, and the more viscous one passively driven by viscous coupling at the interface.

(b) Oscillatory regime: for B smaller than $B_c(\gamma, a)$, the vertical velocity is maximum at the interface (figure 3a) and the pulsation is non-zero (figure 3c); the interface deforms and oscillatory motions develop over the whole box depth (figure 3b). This

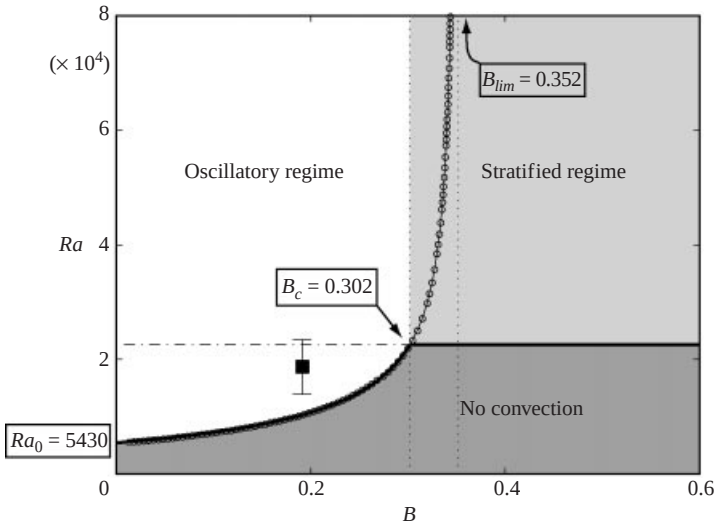

FIGURE 2. Neutral curves of marginal stability analysis in the case $\gamma = 6.7$, $a = 0.5$. Dash-dotted line corresponds to the stratified regime and circles to calculated points of the oscillatory regime (the solid line represents the fit according to 2.25*b*). The bold solid line follows the most unstable regime: in the dark grey domain, no convection develops, whereas in the white domain, the oscillatory regime is the most unstable and in the light grey domain, the stratified regime is the most unstable. The square shows the measured value of experiment 47.

oscillatory instability sets in since the density at the bottom of the lower layer is smaller than the density of the upper layer in spite of the stabilizing jump across the interface (and/or the density at the top of the upper layer is higher than the density of the lower layer). From (2.1) and (2.2),

$$\rho_i = \rho_{i_0} - \alpha\rho_0\Delta T\left(\frac{T_1 - T_0}{\Delta T} - (z + a)\right). \tag{2.22}$$

Thermal effects reverse the chemical density contrast when

$$\rho_1(z) = \rho_2(0) \Leftrightarrow z = -B \text{ (provided } B \leqslant a) \tag{2.23a}$$

and

$$\rho_2(z) = \rho_1(0) \Leftrightarrow z = B \text{ (provided } B \leqslant 1 - a). \tag{2.23b}$$

Thus a Rayleigh–Taylor-type overturning instability operates throughout part of the cycle (figure 1*d*), while dissipative effects (viscous forces and thermal diffusion) together with the stabilizing density contrast across the interface lead to a restoring force throughout the remainder of the cycle. These oscillatory motions can take the form of standing waves if the horizontal dimension of the cell is a multiple of the horizontal wavelength of the flow; otherwise, travelling waves develop. Their critical Rayleigh number increases with B, since the restoring force due to the stable density contrast becomes bigger (figure 2). For the closely related double-diffusive convection case where for example a layer of water with a stabilizing linear salt gradient is heated from below (Veronis 1968; Baines & Gill 1969), the critical Rayleigh number Ra_c scales as

$$Ra_c = Ra_0 + R_s, \tag{2.24}$$

where R_s is the Rayleigh number based on the total chemical density contrast. The

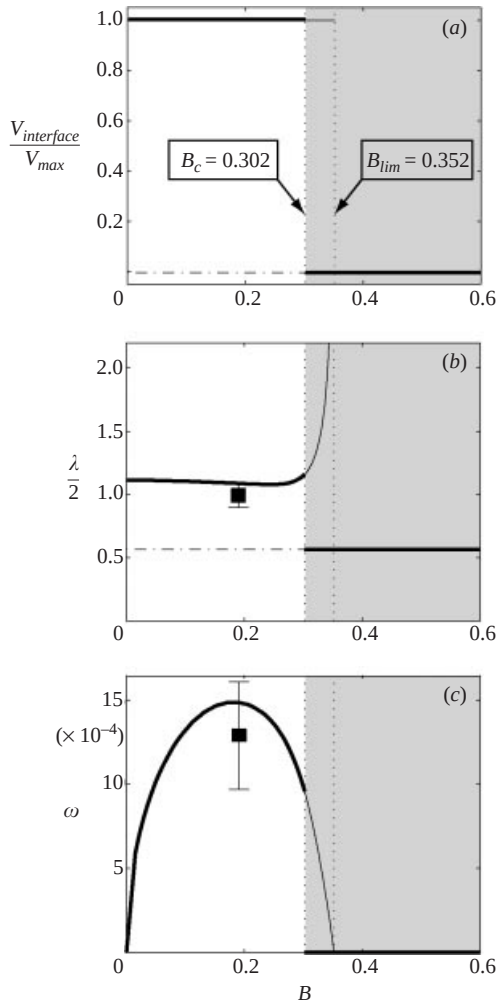

FIGURE 3. (*a*) Ratio of vertical interface velocity to maximum vertical velocity, (*b*) half horizontal wavelength ($\lambda/2 = \pi/k$) and (*c*) temporal frequency for the case $\gamma = 6.7$, $a = 0.5$. Dash-dotted line corresponds to the stratified regime, solid line to the oscillatory regime, and the bold solid line follows the most unstable regime. In the white domain, the oscillatory regime is the most unstable and in the light grey domain, the stratified regime is the most unstable. Squares show measured values of experiment 47.

system is destabilized when there is enough energy to overcome viscous and thermal diffusion effects as in classical Rayleigh–Bénard convection (Ra_0) and to reverse the stabilizing salt gradient (R_s). Although we have a chemical density jump at the interface instead of a linear salinity gradient, we find a similar dependence and the results are well-fitted by

$$Ra_c = Ra_0 + \beta R_s, \tag{2.25a}$$

where β is a constant. Using (2.17),

$$Ra_c = \frac{Ra_0}{1 - B/B_{lim}}, \tag{2.25b}$$

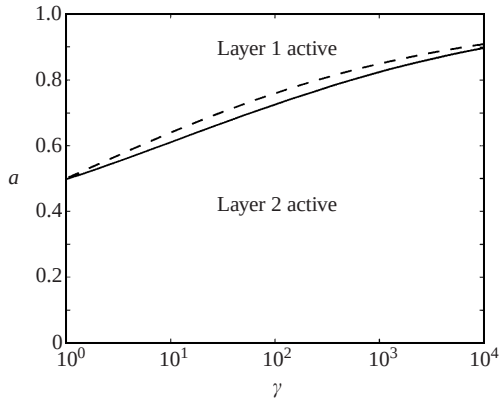

FIGURE 4. Active layer in the stratified regime. The solid line shows the effective transition and the dashed line corresponds to $Ra_1 = Ra_2$.

where $B_{lim} = 1/\beta$ (figure 2). The two constants entering (2.25*b*) are function of a and γ. $B_{lim}(\gamma, a)$ corresponds to the point where the chemical stratification becomes too important to be reversed by any thermal effect, and so the oscillatory regime disappears ($Ra_c \to \infty$). $Ra_0(\gamma, a)$ corresponds to the limit where B tends towards 0, and the oscillatory mode transforms itself into the classical steady ($\omega \to 0$) whole layer mode with a viscosity jump, since no chemical stratification acts against the thermal destabilization.

2.2.3. *Influence of a and* γ

(*a*) Stratified regime: the stratified regime is independent of the buoyancy ratio B. Therefore, the individual Rayleigh numbers of each layer are helpful to describe the dynamics:

$$Ra_1 = \frac{a^4}{\gamma} Ra \quad \text{and} \quad Ra_2 = (1-a)^4 Ra. \tag{2.26}$$

When the two layers have the same thickness ($a = 0.5$), the onset of convection is determined by the layer with the greater Rayleigh number, as already shown by Rasenat *et al.* (1989). When the depth ratio $a \neq 0.5$, the active layer (i.e. where the velocity is maximum) is not always the one with the higher Rayleigh number Ra_i, for it is easier for a viscous layer to entrain a less viscous layer than the reverse (figure 4).

In all cases, the convective motion wavelength is, at first order, proportional to the thickness of the active layer (figure 5*b*). Convection in the other layer is passive, being viscously driven only, and becomes more and more sluggish as the viscosity ratio increases. As γ becomes infinite (typically $\gamma > 100$), the more viscous layer behaves almost rigidly, and the critical Rayleigh number of the system increases towards an asymptotic value which corresponds to a layer of fluid below a slab of finite conductivity (Nield 1968) (figures 6*a* and 6*c*).

According to marginal stability analysis, the coupling between the two layers is always viscous, irrespective of the vertical temperature profile. For $\gamma = 1$ and $a = 0.5$, the temperature perturbation changes sign at the interface $z = 0$. As γ increases, the depth where the temperature perturbation θ changes sign moves into the most viscous layer, so that for $a = 0.5$ and $\gamma > 5$, the vertical temperature profile is correlated over the whole depth (a situation usually encountered when the two layers are 'thermally coupled') although the motions in the layers are still viscously coupled. To reconcile

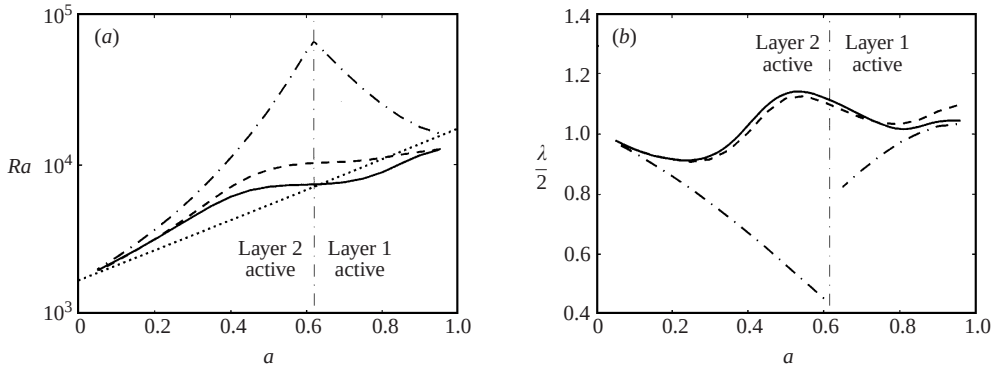

FIGURE 5. (*a*) Critical Rayleigh number and (*b*) half-wavelength as a function of the layer depth ratio for a fixed value of the viscosity ratio ($\gamma = 10$). Dash-dotted lines correspond to the stratified regime, dashed lines to the oscillatory regime when $B = 0.10$ and solid lines to the steady whole-layer regime ($B = 0$). The dotted line represents the fit according to (2.30*a*): in the case $\gamma = 10$, 'vertical' oscillations are predominant for almost all values of the layer depth ratio and the simple law (2.30*a*) reproduces numerical results within 30%.

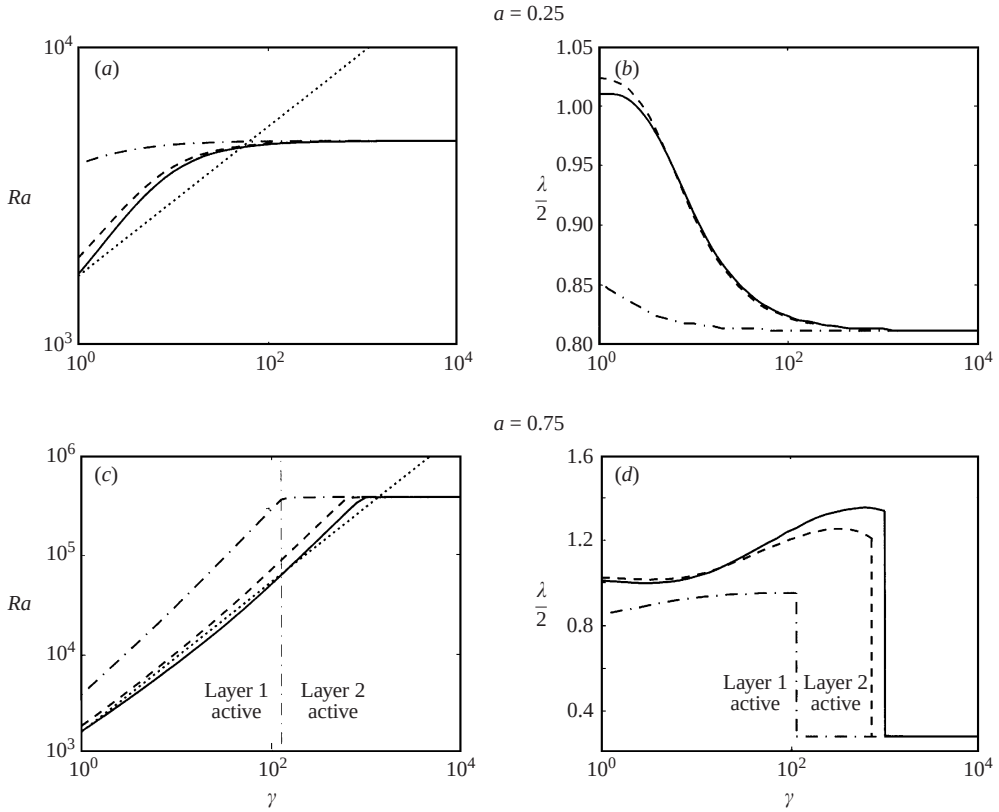

FIGURE 6. (*a*, *c*) Critical Rayleigh number and (*b*, *d*) half-wavelength as a function of the viscosity ratio for fixed values of the layer depth ratio. Dash-dotted lines correspond to the stratified regime, dashed lines to the oscillatory regime when $B = 0.10$ and solid lines to the steady whole-layer regime ($B = 0$). The dotted line represents the fit according to (2.30*a*): in the case $a = 0.75$, 'vertical' oscillations take place for $\gamma < 10^3$ and the simple law (2.30*a*) reproduces numerical results within 30%; on the other hand, for $a = 0.25$, 'horizontal' oscillations take place very rapidly and (2.30*a*) therefore is of no use for $\gamma > 10$.

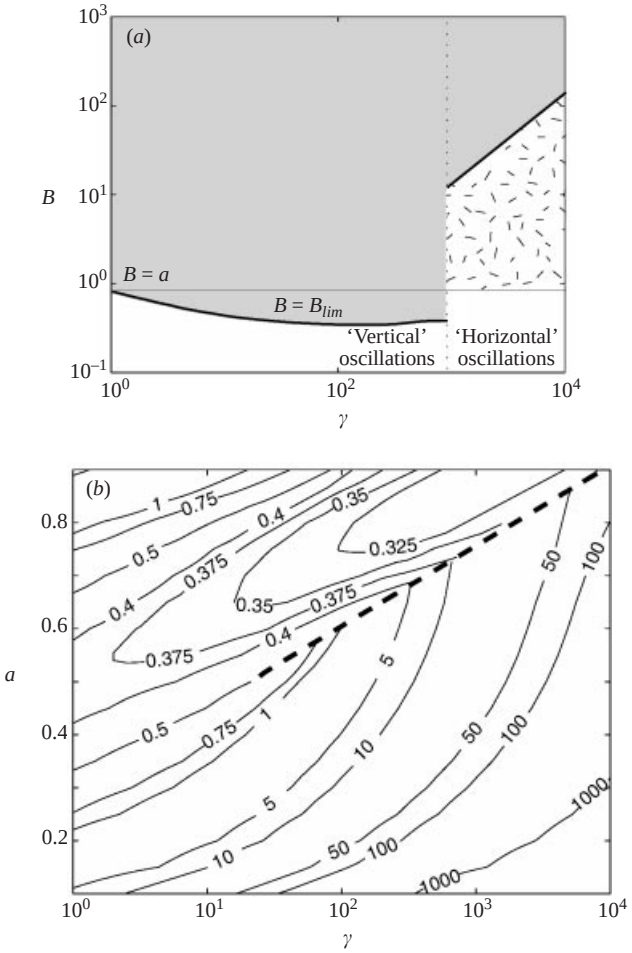

FIGURE 7. (*a*) B_{lim} as a function of the viscosity ratio for $a = 0.75$; the white domain corresponds to oscillations with an unstable whole-layer density profile ($B < a$ or $B < 1 - a$) and the hatched domain to oscillations with a stable whole-layer density profile ($B > a$ and $B > 1 - a$). In the grey domain, oscillations are impossible. (*b*) Contour plot of B_{lim}; the dashed line follows the discontinuity observed in (*a*).

the viscous coupling at the interface with the vertical thermal structure where the temperature perturbation does not change sign throughout the whole tank depth, a third roll sometimes appears in the passive layer. For finite-amplitude perturbations or well above criticality, it is thus expected that both temperature and motions will be thermally coupled for $\gamma > 5$. This has been seen experimentally by Rasenat *et al.* (1989) and in finite-amplitude calculations by Cserepes *et al.* (1988).

(*b*) Oscillatory regime: depending on the value of γ, two types of oscillations can appear, corresponding to two different mechanisms. When the viscosity contrast is not too high, oscillations are due to the opposite effects of chemical and thermal density anomalies, as previously described: the whole-layer density profile is unstable for all values of $B < B_{lim}$ (figure 7), and a Rayleigh–Taylor overturn takes place, leading to convection over the whole depth (figure 8*a*). As a result, the interface velocity is high (figure 9) and the horizontal wavelength comparable to the tank thickness (figures 5*b*, 6*b* and 6*d*). These whole depth convective oscillations will be referred to

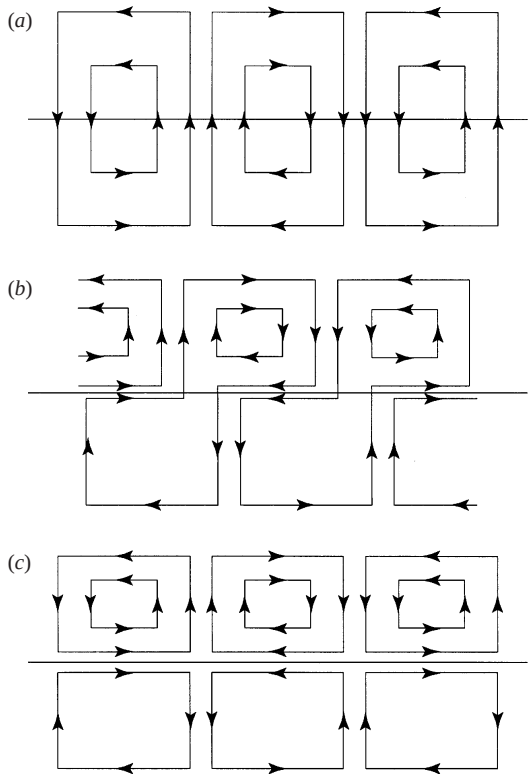

FIGURE 8. Sketch of streamlines in the case of (*a*) 'vertical' oscillations, (*b*) 'horizontal' oscillations and (*c*) stratified regime.

as 'vertical' oscillations. In this case, it is interesting to define an equivalent viscosity of the two-fluid system, for instance

$$v_{eq} \sim v_1^a \times v_2^{1-a} \tag{2.27}$$

and an equivalent Rayleigh number

$$Ra_{eq} = Ra\frac{v_2}{v_{eq}} \sim Ra \times \gamma^{-a}. \tag{2.28}$$

When chemical effects vanish ($B = 0$), convection in the two-layer system is identical to the classical convection in the one-fluid equivalent system: according to Chandrasekhar (1961), the onset is defined by

$$Ra_{eq} = 1707.76. \tag{2.29}$$

This means for the two-layer system

$$Ra_0 \sim 1707.76 \times \gamma^a \tag{2.30a}$$

and using (2.25*b*),

$$Ra_c \sim \frac{1707.76}{1 - B/B_{lim}} \times \gamma^a. \tag{2.30b}$$

Although the values of Ra_0 calculated from the complete resolution of (2.7)–(2.21) span over two orders of magnitude, (2.30*a*) predicts them within 30% (figures 5*a*

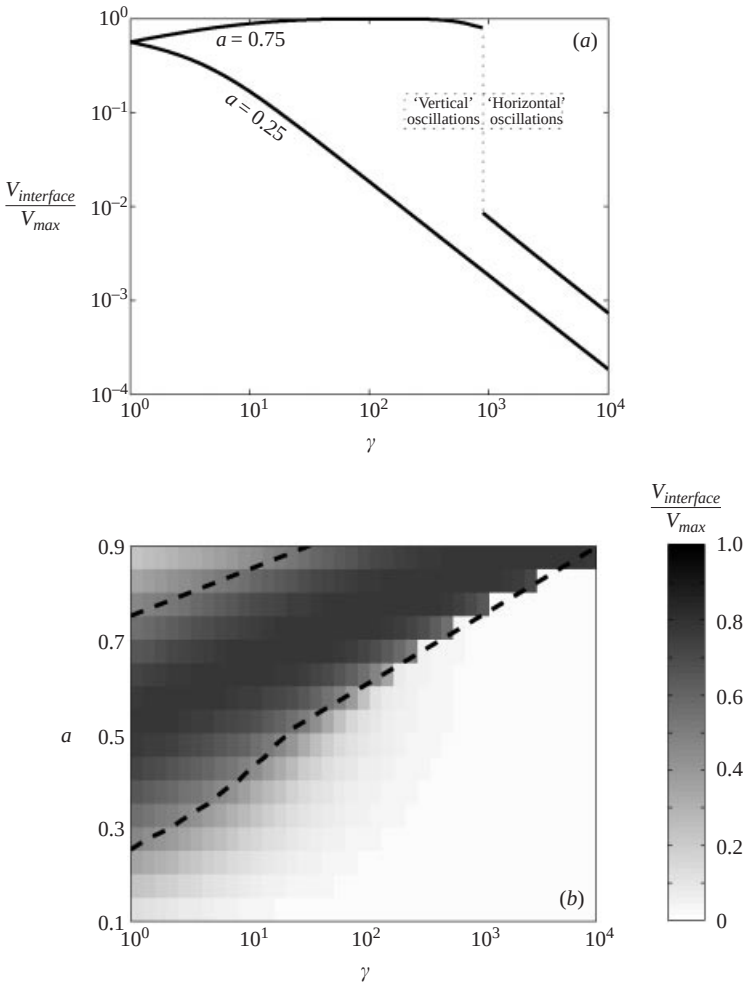

FIGURE 9. Ratio of vertical interface velocity to maximum vertical velocity (a) for two fixed values of layer depth ratio and (b) over the whole range of viscosity and layer depth ratios. The dashed line corresponds to $B_{lim} = \max(a, 1-a)$: low interface velocities are systematically associated with stable whole-layer density profiles.

and 6c). The approximations (2.30a) and (2.30b) are valid when 'vertical' oscillations occur, i.e. in the domain of (γ, a) outlined on figure 9(b).

On the other hand, when the viscosity ratio increases, the interface acts like a barrier: vertical motions are deflected, and the streamlines become more and more concentrated in the less viscous layer (figure 8b). This behaviour is reminiscent of thermal convection in a fluid whose viscosity depends strongly on temperature, where convection occurs in a sublayer over which the viscosity ratio is less than 100 (Stengel, Olivier & Broker 1982; Richter, Nataf & Daly 1983; Davaille & Jaupart 1993). The wavelength of the convective pattern thus decreases from a value comparable to the full thickness of the tank to a value comparable to the thickness of layer 2 (figures 6b and 6d): convection does not develop over the whole depth but only in the less viscous layer, the more viscous one being slightly perturbed by thermal coupling at the interface. The system thus tends towards the previously described stratified regime where the less viscous fluid is the active layer: the critical Rayleigh number smoothly

increases towards the asymptotic value for the stratified regime (figures 6*a* and 6*c*), while the time frequency of the oscillations tends towards 0. Moreover, the maximum vertical velocity scales as the typical convective velocity in layer 2

$$V_{max} \sim \frac{\alpha g \Delta T_2 d_2^2}{\nu_2}, \tag{2.31}$$

where ΔT_2 is the temperature difference across layer 2, whereas the interface velocity is limited by the penetration of this thermal instability in the viscous layer, thus scaling as

$$V_{interface} \sim \frac{\alpha g \Delta T_2 d_2^2}{\nu_1}. \tag{2.32}$$

As a result, the ratio $V_{interface}/V_{max}$ rapidly decreases as γ^{-1} (figure 9*a*). Simultaneously, B_{lim} significantly increases and becomes larger than a and $1-a$: oscillations are possible with a stable whole-layer density profile (figure 7). Oscillations still exist because of the opposite effects of thermal and viscous coupling that decorrelate horizontal motions around the interface. The mechanism of these 'horizontal' oscillations is thus comparable to the oscillatory coupling instabilities described by Rasenat *et al.* (1989) in the absence of interface deformation.

The transition between 'vertical' and 'horizontal' oscillations is continuous for $a \leqslant 0.5$ (figures 6*a* and 6*b*). In this case, motion in the less viscous thicker layer slightly precedes motion in the other one: it thus initiates oscillations, which are progressively confined as γ increases. For $a \geqslant 0.5$, the transition is sharp (figures 6*c* and 6*d*). 'Vertical' oscillations are first initiated by the viscous thicker layer, but as γ increases, this fluid becomes too rigid to move: 'horizontal' oscillations initiated by the other fluid then take place.

When a tends towards 0 or 1, the proximity of the outer boundary prevents the interface from oscillating, and the oscillatory mode transforms itself into the classical steady ($\omega \to 0$) one-layer mode. As shown in figure 5, the wavenumber tends towards 3.12, corresponding to $\lambda/2 \approx 1$, whereas Ra_c tends towards 1707.76 for $a \to 0$ and towards $1707.76 \times \gamma$ for $a \to 1$ (because our scaling uses the viscosity of layer 2).

2.3. *Development of the oscillatory regime*

Besides marginal stability, it is also interesting to determine the behaviour of the most unstable oscillatory mode for given γ, a, B, Ra. In this case, the roots of the determinant are now sought in the (σ, ω) space, the wavenumber k being fixed to the value determined by marginal stability. Starting from the neutral curve and increasing Ra, we observe that the growth rate σ progressively increases, whereas the frequency of the oscillations ω rapidly decreases and finally vanishes for $Ra > Ra_{lim}(B)$ (figure 10): thermal effects are then high enough permanently to reverse the chemical stratification, and the oscillatory regime is transformed into a steady whole-layer mode, as already noted when $B = 0$.

3. Laboratory experiments

3.1. *Experimental set-up*

We performed laboratory experiments in which two superimposed layers of viscous fluids, initially isothermal at T_0, are suddenly cooled from above and heated from below. The fluids are mixtures of water, salt for density control and cellulose for viscosity control. The density, viscosity and depth of each fluid as well as the boundary

γ	a	B	Ra
1 to 6×10^4	0.03 to 0.97	0.048 to 4.4	6.7×10^3 to 6.1×10^8
$\pm 50\%$	$\pm 5\%$	$\pm 1\%$	$\pm 25\%$

TABLE 1. Range and accuracy of experiments dimensionless numbers.

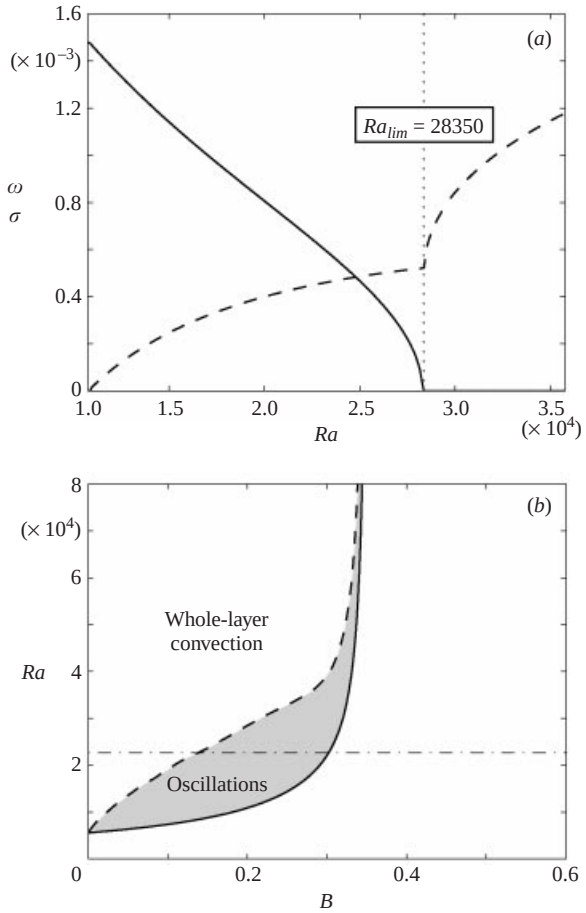

FIGURE 10. Development of the oscillatory regime in the case $\gamma = 6.7$, $a = 0.5$. (a) Evolution of the temporal periodicity ω (solid line) and the growth rate σ (dashed line) when Ra is progressively increased from the marginal stability value at $B = 0.20$. (b) Boundary between oscillatory and whole-layer regimes: the solid line corresponds to the neutral curve of the oscillatory regime and the dashed line to $Ra = Ra_{lim}(B)$. The neutral curve of the stratified regime is also reported (dash-dotted line).

temperatures are measured for each experiment, in order to determine the characteristic dimensionless numbers. Variation ranges and accuracy are listed in table 1. The only major uncertainty comes from the viscosity measurements (accuracy of 25%). However, as demonstrated by the linear study, changes in γ over the error range have a minor influence on the dynamics. Prandtl numbers in each layer are always greater than 100 to ensure that inertial effects are non-existent (Krishnamurti 1970). The liquids are miscible in all proportions and the temperature-dependence of the

Exp. number	γ	a	B	B_c	Ra	$Ra_c(B)$	$Ra_{lim}(B)$	Behaviour
2	12.5	0.5	0.26	0.28	2.2×10^4	2.1×10^4	3.3×10^4	osc.
3	12	0.5	0.18	0.28	5.2×10^4	1.4×10^4	3.0×10^4	whole layer
7	149	0.75	0.24	0.25	4.2×10^5	2.9×10^5	4.3×10^5	osc.
45	1.3	0.44	0.10	0.32	6.8×10^3	2.7×10^3	6.6×10^3	whole layer
46	1.1	0.44	0.048	0.32	6.7×10^3	2.0×10^3	4.0×10^3	whole layer
47	6.7	0.5	0.20	0.30	1.8×10^4	1.1×10^4	2.8×10^4	osc.

TABLE 2. Dimensionless parameters and behaviour of the experiments close to marginal stability. B_c and $Ra_c(B)$ are the theoretical values of critical buoyancy and Rayleigh numbers; $Ra_{lim}(B)$ is the calculated value where oscillations are replaced by steady whole-layer convection (see § 2.3).

viscosity is negligible compared to its composition-dependence. The high viscosities render diffusion of salt across the interface extremely slow compared to the characteristic time scale of the instabilities (Davaille 1999*a*). Moreover, to be able to compare the experimental results with the linear stability analysis, we consider here only the experiments where the initial density stratification is sharp. Heat and mass transfer are monitored over time by measuring temperature profiles and the densities of both layers. More details can be found in Davaille (1999*a*).

Since the fluids are miscible in all proportions, slow mixing by mechanical entrainment occurs through the interface and the characteristics of convection (thermal structure, regime, etc.) evolve through time, from two-layer to classical Rayleigh–Bénard convection. However, typical mixing times are at least one order of magnitude greater than thermochemical time scales. We focus hereafter on the early stages of the experiments.

3.2. *Close to marginal stability*

Six of our experiments were close to marginal stability (see table 2). Since the stratified case is well-documented (Richter & McKenzie 1981; Busse 1981; Cserepes & Rabinowicz 1985; Ellsworth & Schubert 1988; Cserepes *et al.* 1988; Sotin & Parmentire 1989), we concentrated on the oscillatory regime. The onset of all experiments is always the same. First a linear temperature profile progressively sets in the tank by heat diffusion: the thermal structure at onset is thus exactly the same as our theoretical study. Provided $Ra > Ra_c(B)$, convection then begins and the interface deforms in large domes with a horizontal wavelength comparable to twice the tank depth (figure 11*a*), as predicted by the marginal stability analysis (figure 3*b* and table 3). These domes progressively rise, and finally reach the cold plate where they begin to cool down and become heavier. Two behaviours can then occur:

(i) When domes do not spread under the cold plate, no large-scale stirring operates: the two fluids remain separate, and oscillations begin (figure 11*b*). Large temperature variations are recorded. Their periodicities are in good agreement with the theory (figure 3*c* and table 3). Only travelling waves are observed, because the horizontal dimension of our tank is not a multiple of the horizontal wavelength of the flow (tank 30 cm wide for typical periodicities of 12 cm or 16 cm).

(ii) When domes spread under the cold plate, stirring operates from the first oscillation: fluid 1 sinks back while entraining part of the other fluid, leading to a spiral pattern (figure 11*c*). Steady convection thus takes place over the whole depth of the tank. However, we observed in oscillatory experiments that the temperature

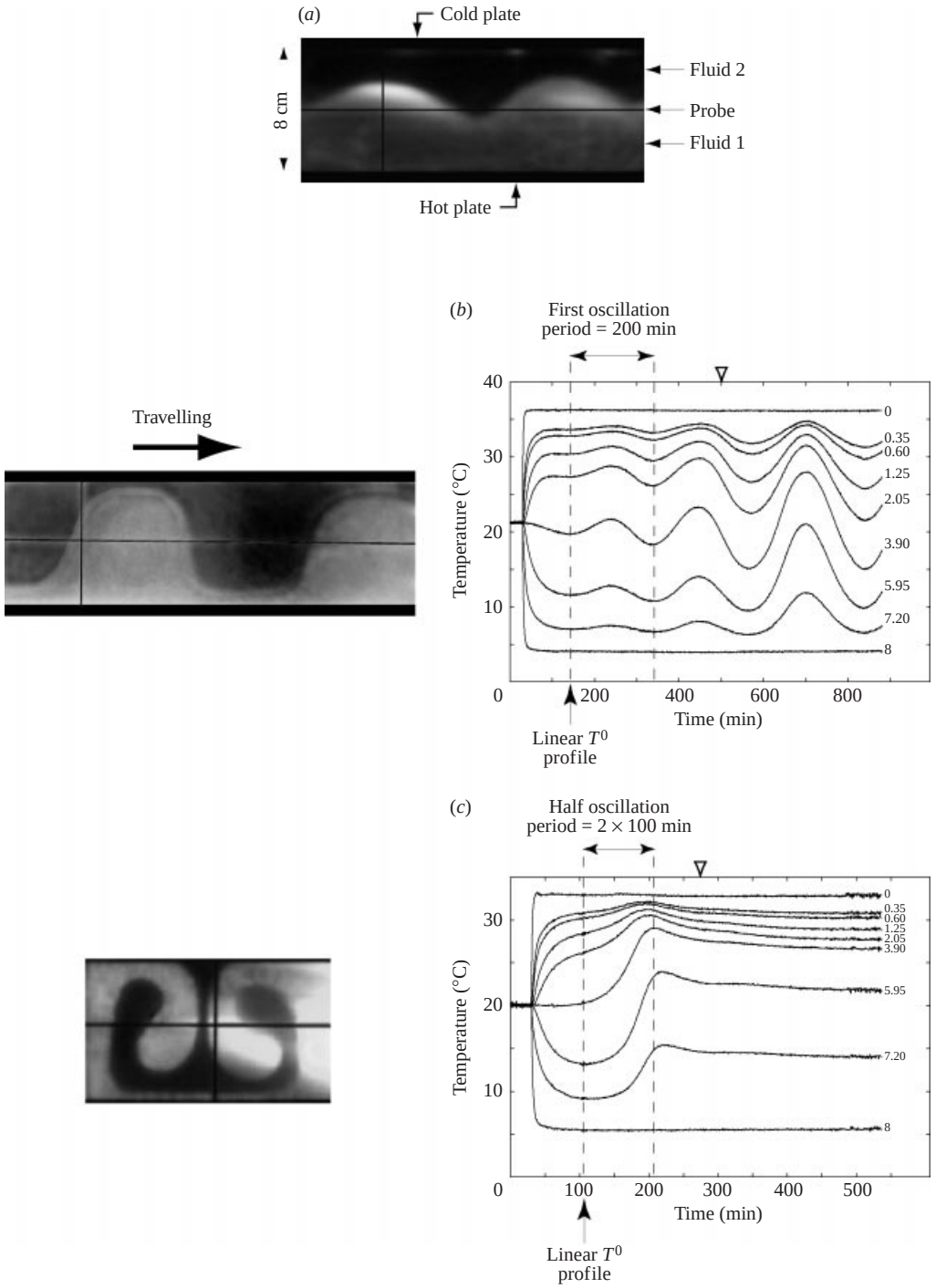

FIGURE 11. (*a*) Onset of convection, characteristic of all experiments close to marginal stability. (*b*) Picture and vertical temperature signal of experiment 47, where travelling waves were observed during more than 24 hours and (*c*) the same for experiment 46, where whole-layer convection took place. Positions of the vertical thermocouples (in cm) are reported in the right of the temperature signals and triangles show the time when photos were taken.

Exp. number	$\lambda_e/2$	$\lambda_{ms}/2$	ω_e	ω_{ms}
2	1.1	1.1	8.5×10^{-4}	7.8×10^{-4}
3	1.1	1.1	9.0×10^{-4}	9.3×10^{-4}
7	1.0	0.98	8.4×10^{-5}	7.6×10^{-5}
45	0.91	1.0	3.4×10^{-3}	3.6×10^{-3}
46	0.93	1.0	3.3×10^{-3}	3.1×10^{-3}
47	1.0	1.1	1.3×10^{-3}	1.5×10^{-3}

TABLE 3. Horizontal wavelengths and temporal frequencies of the experiments close to marginal stability. Subscript *e* stands for experimental values, and *ms* for marginal stability. Temporal frequencies are determined using the temperature signal in the tank; for spiral patterns, a virtual period is deduced from the first half of the oscillation (accuracy $\pm 25\%$). Horizontal wavelengths are determined using an horizontal temperature profile at the beginning of interface deformation (accuracy $\pm 10\%$).

signal is symmetrical (figure 11*b*): the time for domes to rise is equal to half a period. So one can deduce from the temperature signal of steady whole-layer experiments an extrapolated temporal periodicity, which also shows good agreement with the theoretical value (table 3).

Which behaviour will actually prevail depends on the relative values of thermal and chemical density anomalies, as already described in § 2.3: when thermal effects are strong compared to chemical stratification (high Ra or small B), whole-layer convection takes place instead of oscillations.

Care is required to extrapolate the linear study results to experiments, in particular because of the theoretical assumption that the interface deformation remains small. But it is noticeable that the mode excited in these experiments is exactly the one determined by the marginal stability analysis. Moreover, the further development of the selected mode is also predicted: the calculated values of Ra_{lim} separating whole-layer convection from oscillations are in good agreement with observations (table 2). This was also observed by Schmeling (1988) in numerical simulations for $\gamma = 1$, $a = 0.5$ (figure 12).

3.3. *Stability of two-layer convection*

When the Rayleigh number is high compared to the critical value, finite-amplitude effects are so important that typical scales of convection can no longer be derived from the marginal stability analysis. However, the two convective regimes are still observed (Olson & Kincaid 1991; Davaille 1999*b*): we can thus use the linear theory to solve two problems for each experiment, namely which regime develops first and which regime remains once the temperature gradient is established.

3.3.1. *Onset of instability*

The thermal structure at $t = 0$ in our tank is different from the initial linear temperature profile of the marginal stability: in the experiments, the two fluids are initially at the same temperature T_0, and then suddenly heated from below and cooled from above. Thermal boundary layers subsequently grow symmetrically from the hot and cold plates, until the first convective feature appears. We observed two types of onset:

(*a*) the deformation of the interface over a large scale (several centimetres), corresponding to the oscillatory regime;

(*b*) the appearance of small (less than one centimetre) short-lived plumes coming

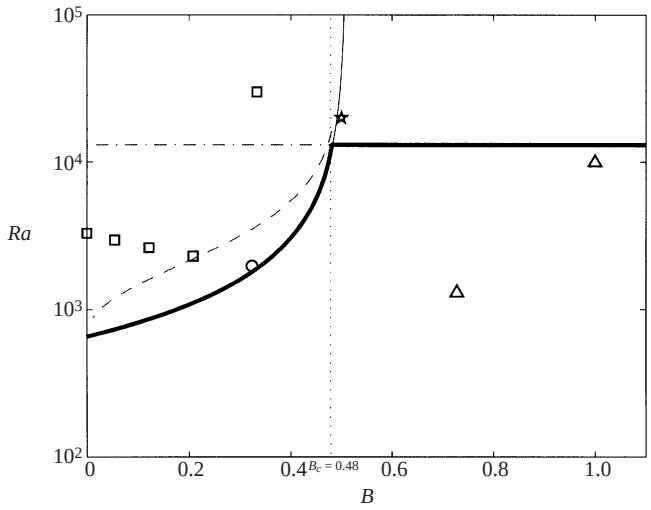

FIGURE 12. Numerical simulations by Schmeling (1988) for $\gamma = 1$, $a = 0.5$: squares correspond to whole-layer convection, the star to the stratified regime, the circle to oscillations and triangles to no convection. Results of the linear study are also reported: the dash-dotted line corresponds to the stratified regime, the solid line to the oscillatory regime. The bold solid line follows the most unstable regime and the dashed line $Ra = Ra_{lim}(B)$.

from the destabilization of one of the outer thermal boundary layers (Olson 1984; Davaille 1999*a*). Those plumes correspond to thermal convection in a sublayer, and thus to the stratified regime.

In order to follow the evolution of the experiment during the setting of the temperature gradient, we can calculate an effective Rayleigh number based on the typical length scale of thermal effects

$$Ra_{eff} = \frac{\alpha g \Delta T (2\delta)^3}{\kappa \nu_2} = Ra \left(\frac{2\delta}{d} \right)^3, \tag{3.1}$$

where δ is the theoretical size of a thermal boundary layer growing by conduction. Since the chemical stratification is already established over the whole tank depth (fixed R_s), the corresponding effective buoyancy number is

$$B_{eff} = \frac{R_s}{Ra_{eff}} = B \left(\frac{d}{2\delta} \right)^3. \tag{3.2}$$

In the (B, Ra) space, the experiment thus follows the curve

$$Ra_{eff} = Ra \frac{B}{B_{eff}}, \tag{3.3}$$

and the onset of convection is determined by the first intersection of this curve with the curve of marginal stability (figure 13). The oscillatory regime can be triggered when $Ra \geqslant Ra_c(B)$, and the intersection corresponds to

$$Ra_{eff} = Ra_c(B_{eff}). \tag{3.4}$$

This means, using (2.25*b*),

$$Ra_{eff} = Ra_0 + \frac{B}{B_{lim}} Ra \Leftrightarrow \delta_{osc} = \frac{d}{2} \left(\frac{Ra_0}{Ra} + \frac{B}{B_{lim}} \right)^{1/3}. \tag{3.5}$$

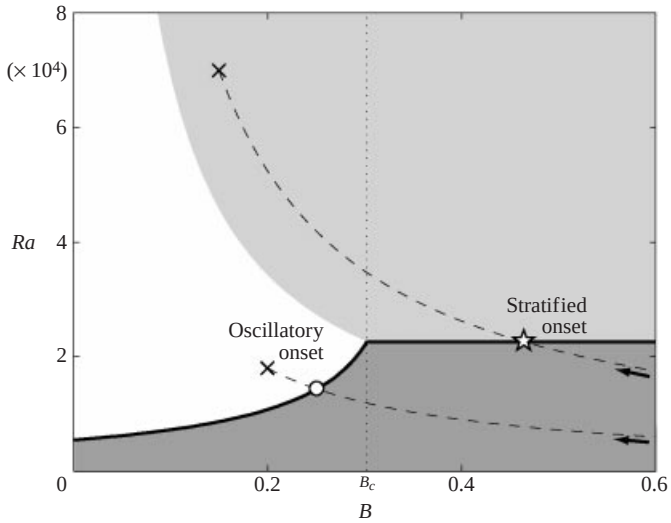

FIGURE 13. Onset of convection in the (B, Ra) space for $\gamma = 6.7$, $a = 0.5$. In the dark grey domain no convection develops, whereas in the white domain the oscillatory regime sets in first and in the light grey domain the stratified regime sets in first. The dashed lines represent the time evolution of two possible experiments during the setting of the temperature gradient: the onset of convection corresponds to their first intersection with the neutral curve of marginal stability (bold solid line).

The stratified regime can be triggered when $Ra \geqslant Ra_{strat}$, and the intersection corresponds to

$$Ra_{eff} = Ra_{strat} \Leftrightarrow \delta_{strat} = \frac{d}{2}\left(\frac{Ra_{strat}}{Ra}\right)^{1/3}. \tag{3.6}$$

We can however notice that for very large values of layer Rayleigh number ($Ra_i > 10^5$ typically), the corresponding thermal boundary layer will be destabilized before 'seeing' the interface and the second fluid, following Howard's mechanism for purely thermal plumes (Howard 1964): the onset will thus be given by

$$\delta_{strat} = d_i\left(\frac{1100.67}{Ra_i}\right)^{1/3}. \tag{3.7}$$

Since the thermal boundary layer initially grows by conduction, the first convective motion corresponds to the smallest δ. Depending on the relative value of B and Ra, this defines three different domains (figure 13):

no convection when $Ra < Ra_{strat}$ and $Ra < Ra_c(B)$;
oscillatory regime sets in first when $\delta_{osc} < \delta_{strat}$;
stratified regime sets in first when $\delta_{osc} > \delta_{strat}$.

All experiments agree well with this model, independently of the relative value of B and B_c (figure 14). The convective history of each experiment must thus be divided into two independent steps: first, the temperature gradient is progressively established over the tank depth, and effective values (B_{eff}, Ra_{eff}) determine which regime starts first; but as soon as this convective motion appears, (B_{eff}, Ra_{eff}) are meaningless, and global values (B, Ra) must be used.

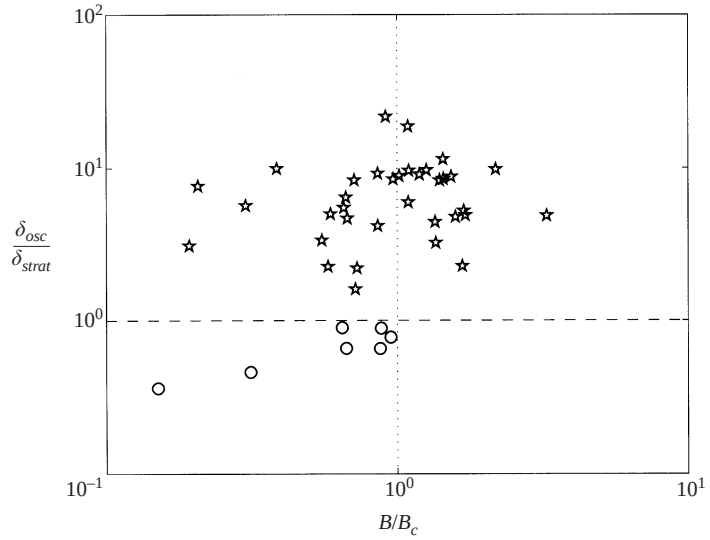

FIGURE 14. Observed onset for all experiments as a function of the ratio $\delta_{osc}/\delta_{strat}$. Stars correspond to experiments where small plumes start first (stratified regime), and circles to experiments where large domes start first (oscillatory regime).

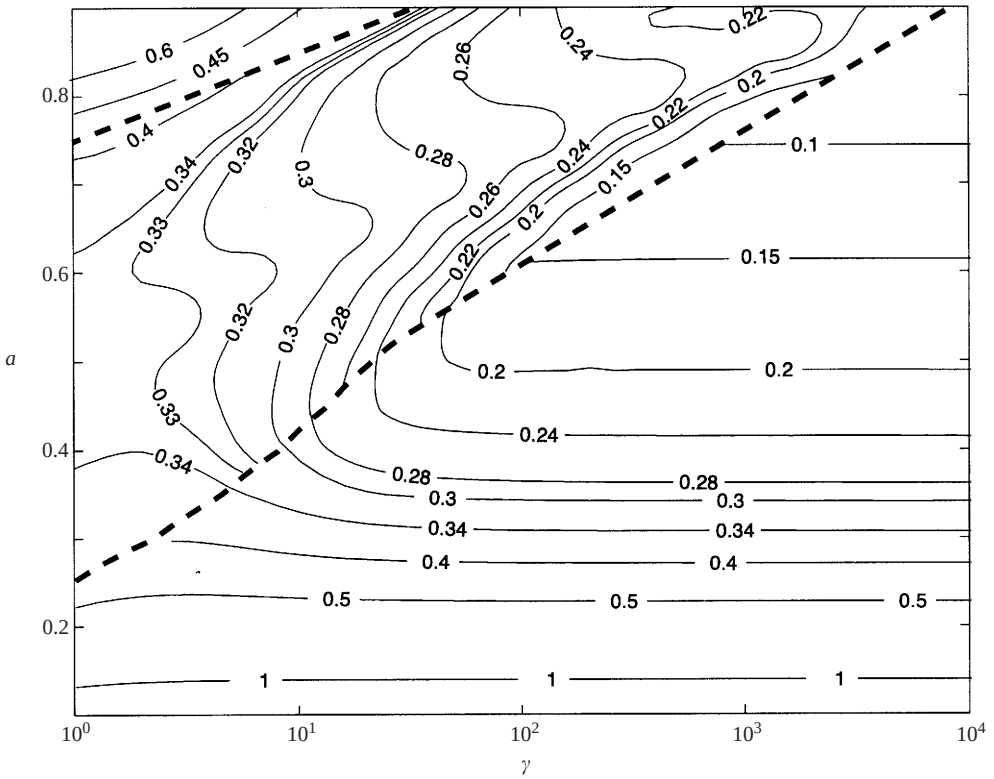

FIGURE 15. Calculated $B_c(\gamma, a)$ over the whole parameter space. The dashed line corresponds to $B_{lim} = \max(a, 1-a)$, thus to the limit between 'vertical' and 'horizontal' oscillations (see § 2.2.3).

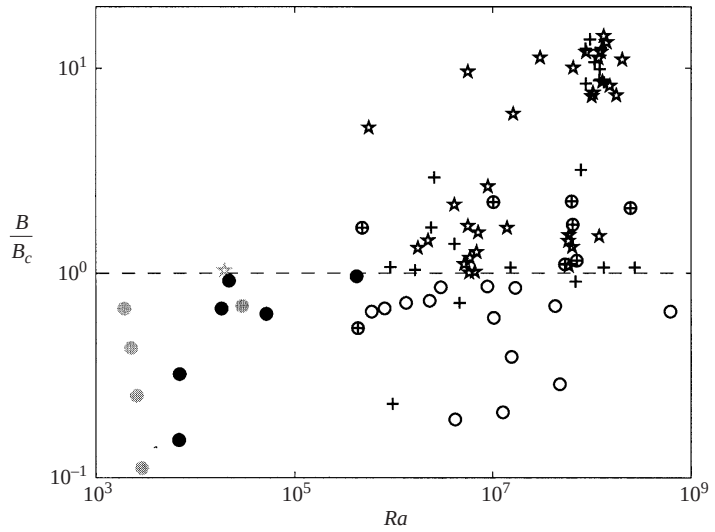

FIGURE 16. Observed persistent regime as a function of the ratio B/B_c. Experiments corresponding in marginal stability to 'vertical' oscillations are shown by stars when the interface remains stable and circles when the interface deforms in large domes (open circles denote experiments where domes appear after a stratified onset). Experiments corresponding in marginal stability to 'horizontal' oscillations are shown by crosses when the interface remains stable and cross-circles when the interface deforms in large domes. Numerical simulations by Schmeling (1988) are also reported in grey.

3.3.2. *Oscillatory whole-layer versus steady stratified regimes*

According to the linear stability analysis, which thermochemical regime is the most unstable depends on the relative value of the buoyancy number B and the critical buoyancy number $B_c(\gamma, a)$ (figure 2). In the experiments, once the convection has begun, we can thus try to determine whether the interface will be deformed or not by comparing the values of the experimental B and the theoretical $B_c(\gamma, a)$ (figure 15). Figure 16 shows for all experiments the nature of the observed regime depending on the ratio $B/B_c(\gamma, a)$. The agreement between theory and observations is quite good, except for some points corresponding in marginal stability to 'horizontal' oscillations (see § 2.2.3): this is due to the difficulty in extrapolating linear theory results to experiments. We can reasonably suppose that 'vertical' oscillations characterized in the linear study by high interface velocities and whole-layer instable density profiles will effectively lead to the formation of large domes over the whole tank depth: indeed, all corresponding experiments agree well with the theory. However, in the case of 'horizontal' oscillations, which are due to opposite effects of viscous and thermal coupling, the linear theory predicts low interface velocities as well as stable whole-layer density profiles: a finite-amplitude study would thus be necessary to know whether the predicted interface oscillations will give rise to an effective large-scale deformation, but this is beyond the scope of this paper.

We can however notice that the theoretical B_c for 'vertical' oscillations varies in the limited range 0.2–0.4 over the whole parameter space (figure 15). These typical values also seem to be relevant for the experiments with large viscosity contrast and/or a thin layer, where 'vertical' oscillations are observed experimentally for B between 0.093 and 0.33, whereas the interface remains stable for B larger than 0.32.

4. Conclusion

The influence of a contrast in viscosity on the linear stability of two-layer thermal convection in the presence of stable density stratification has been investigated. Depending on the buoyancy number, the ratio of the stabilizing chemical density anomaly to the destabilizing thermal density anomaly, two regimes are found: (i) for $B < B_c(\gamma, a)$, an oscillatory regime where vertical motion exists at the interface; and (ii) for $B > B_c(\gamma, a)$, a steady two-layer regime where there is no vertical motion at the interface. Laboratory experiments agree well with this simple rule, even at high Rayleigh number. In the experiments however, the initial convective regime can be different from the final state, since the temperature gradient responsible for the thermal density contrast is progressively imposed on initially isothermal fluids, whereas the chemical density contrast is already present. During this transient state, local values of the parameters must be used.

This study has focused on the early stages of the experiments, but since the fluids are miscible, the characteristics of convection evolve through time. The description of the stratified regime can be found in Davaille (1999*a*); the next problem is thus fully to describe the behaviour of oscillatory domes as well as the mixing between the two layers. It is however already apparent that even density contrasts smaller than 1% can radically change the dynamics of convection, particularly if it is coupled with a viscosity contrast.

This work benefited from fruitful discussions with George Veronis, Neil Ribe, Claude Jaupart, Peter Molnar, Jeffrey Park and Harro Schmeling, and from the constructive comments of three anonymous reviewers. A. D. is grateful to Yale University for its hospitality. This research has been supported by the French INSU programs IDYL and IT. This is an IPGP contribution.

Appendix. Determinant for rigid boundaries

A homogeneous system of twelve equations in twelve unknowns is obtained by substituting the expansions (2.20) into the boundary conditions (2.7)–(2.8) and (2.10)–(2.15). The coefficient matrix is

$$\begin{vmatrix}
1 & 0 \\
\pm q_{1j} & 0 \\
(q_{1j}^2 - k^2)^2 & 0 \\
0 & 1 \\
0 & \pm q_{2j} \\
0 & (q_{2j}^2 - k^2)^2 \\
\mathrm{e}^{\pm q_{1j} a} & -\mathrm{e}^{\pm q_{2j}(1-a)} \\
\pm q_{1j}\,\mathrm{e}^{\pm q_{1j} a} & \pm q_{2j}\,\mathrm{e}^{\pm q_{2j}(1-a)} \\
\gamma(q_{1j}^2 + k^2)\,\mathrm{e}^{\pm q_{1j} a} & -(q_{2j}^2 + k^2)\,\mathrm{e}^{\pm q_{2j}(1-a)} \\
\pm q_{1j} s\gamma(q_{1j}^2 - 3k^2)\,\mathrm{e}^{\pm q_{1j} a} & (\pm q_{2j} s(q_{2j}^2 - 3k^2) - k^2 B)\,\mathrm{e}^{\pm q_{2j}(1-a)} \\
\gamma(q_{1j}^2 - k^2)^2\,\mathrm{e}^{\pm q_{1j} a} & -(q_{2j}^2 - k^2)^2\,\mathrm{e}^{\pm q_{2j}(1-a)} \\
\pm q_{1j}\gamma(q_{1j}^2 - k^2)^2\,\mathrm{e}^{\pm q_{1j} a} & \pm q_{2j}(q_{2j}^2 - k^2)^2\,\mathrm{e}^{\pm q_{2j}(1-a)}
\end{vmatrix}$$

Each column in this matrix actually corresponds to six columns: the coefficients of the first column with the '+' sign correspond to unknowns $A_{1j}, 1 \leqslant j \leqslant 3$, and with the '−' sign to $B_{1j}, 1 \leqslant j \leqslant 3$; the coefficients of the second column with the '+' sign correspond to $A_{2j}, 1 \leqslant j \leqslant 3$, and with the '−' sign to $B_{2j}, 1 \leqslant j \leqslant 3$.

REFERENCES

Andereck, C. D., Colovas, P. W. & Degen, M. M. 1996 Observations of time-dependent behavior in the two-layer Rayleigh–Bénard system. In *Advances in Multi-Fluid Flows* (ed. Y. Y. Renardy, A. V. Coward, D. Papageorgiou & S. M. Sun). SIAM.

Baines, P. G. & Gill, A. E. 1969 On thermohaline convection with linear gradients. *J. Fluid Mech.* **37**, 289–306.

Busse, F. H. 1981 On the aspect ratio of two-layer mantle convection. *Phys. Earth Planet. Inter.* **24**, 320–324.

Busse, F. H. & Sommermann, G. 1996 Double-layer convection: a brief review and some recent experimental results. In *Advances in Multi-Fluid Flows* (ed. Y. Y. Renardy, A. V. Coward, D. Papageorgiou & S. M. Sun). SIAM.

Chandrasekhar, S. 1961 *Hydrodynamic and Hydromagnetic Stability*. Dover.

Cserepes, L. & Rabinowicz, M. 1985 Gravity and convection in a two-layered mantle. *Earth Planet. Sci. Lett.* **76**, 193–207.

Cserepes, L., Rabinowicz, M. & Rosemberg-Borot, C. 1988 Three-dimensional infinite Prandtl number convection in one and two layers with implications for the Earth's gravity field. *J. Geophys. Res.* **93**, 12009–12025.

Davaille, A. 1999*a* Two-layer thermal convection in miscible fluids. *J. Fluid Mech.* **379**, 223–253.

Davaille, A. 1999*b* Simultaneous generation of hotspots and superswells by convection in a heterogeneous planetary mantle. *Nature* **402**, 756–760.

Davaille, A. & Jaupart, C. 1993 Transient high-Rayleigh number thermal convection with large viscosity variations. *J. Fluid Mech.* **253**, 141–166.

Ellsworth, K. & Schubert, G. 1988 Numerical models of thermally and mechanically coupled two-layer convection of highly viscous fluids. *Geophys. J.* **93**, 347–363.

Hansen, U. & Yuen, D. A. 1989 Subcritical double-diffusive convection at infinite Prandtl number. *Geophys. Astroph. Fluid Dyn.* **47**, 199–224.

Howard, L. N. 1964 Convection at high Rayleigh number. In *Proc. 11th Intl Congr. Appl. Mech.* (ed. H. Görtler), pp. 1109–1115. Springer.

Joseph, D. D. & Renardy, M. 1993 *Fundamentals of Two-Fluids Dynamics*. Springer.

Krishnamurti, R. 1970 On the transition to turbulent convection. *J. Fluid Mech.* **42**, 295–320.

Nelder, J. A. & Mead, R. 1965 A simplex method for function minimization. *Computer J.* **7**, 308–313.

Nield, D. A. 1968 The Rayleigh–Jeffreys problem with boundary slab of finite conductivity. *J. Fluid Mech.* **32**, 393–398.

Olson, P. 1984 An experimental approach to thermal convection in a two-layered mantle. *J. Geophys. Res.* **89**, 11293–11301.

Olson, P. & Kincaid, C. 1991 Experiments on the interaction of thermal convection and compositional layering at the base of the mantle. *J. Geophys. Res.* **96**, 4347–4354.

Olson, P., Silver, P. G. & Carlson, R. W. 1990 The large scale structure of convection in the Earth's mantle. *Nature* **344**, 209–215.

Rasenat, S., Busse, F. H. & Rehberg, I. 1989 A theoretical and experimental study of double-layer convection. *J. Fluid Mech.* **199**, 519–540.

Renardy, M. & Renardy, Y. 1985 Perturbation analysis of steady and oscillatory onset in a Bénard problem with two similar liquids. *Phys. Fluids* **28**, 2699–2708.

Renardy, Y. & Joseph, D. D. 1985 Oscillatory instability in a Bénard problem of two fluids. *Phys. Fluids* **28**, 788–793.

Richter, F. M. & Johnson, C. E. 1974 Stability of a chemically layered mantle. *J. Geophys. Res.* **79**, 1635–1639.

Richter, F. M. & McKenzie, D. P. 1981 On some consequences and possible causes of layered convection. *J. Geophys. Res.* **86**, 6133–6142.

Richter, F. M., Nataf, H. C. & Daly, S. F. 1983 Heat transfer and horizontally-averaged temperature of convection with large viscosity variations. *J. Fluid Mech.* **129**, 173–192.

Schmeling, H. 1988 Numerical models of Rayleigh–Taylor instabilities superimposed upon convection. *Bull. Geol. Inst. Univ. Uppsala* **14**, 95–109.

Sotin, C. & Parmentier, E. M. 1989 On the stability of a fluid layer containing a univariant phase transition: application to planetary interiors. *Phys. Earth Planet. Inter.* **55**, 10–25.

Stengel, K. C., Olivier, D. S. & Broker, J. R. 1982 Onset of convection in a variable-viscosity fluid. *J. Fluid Mech.* **120**, 411–431.

Tackley, P. J. 2000 Mantle convection and plate tectonics: toward an integrated physical and chemical theory. *Science* **288**, 2002–2007.

Turner, J. S. 1979 *Buoyancy Effects in Fluids*. Cambridge University Press.

Veronis, G. 1968 Effect of a stabilizing gradient of solute on thermal convection. *J. Fluid Mech.* **34**, 315–336.